



Waste Stream Porous Alkali Activated Materials for High Temperature Application

Diana Bajare, Laura Vitola*, Laura Dembovska and Girts Bumanis

Department of Building Materials and Products, Riga Technical University, Riga, Latvia

OPEN ACCESS

Edited by:

Maria Juenger,
University of Texas at Austin,
United States

Reviewed by:

Sriramya Duddukuri Nair,
Cornell University, United States
Ru Mu,
Hebei University of Technology, China

*Correspondence:

Laura Vitola
laura.vitola_1@rtu.lv

Specialty section:

This article was submitted to
Structural Materials,
a section of the journal
Frontiers in Materials

Received: 18 January 2019

Accepted: 12 April 2019

Published: 22 May 2019

Citation:

Bajare D, Vitola L, Dembovska L and
Bumanis G (2019) Waste Stream
Porous Alkali Activated Materials for
High Temperature Application.
Front. Mater. 6:92.
doi: 10.3389/fmats.2019.00092

The growing interest of using industrial waste as recycled raw materials for the production of new, innovative materials is associated with effective use of natural resources and circular (zero-waste) economy. The research object is waste stream materials coming from chemical and processing industries, such as aluminum scrap recycling waste, chamotte-like precursor, firebricks sawing residues, and their use in production of high-temperature resistant, porous insulation materials by using alkali activation technique with 6 M NaOH solution. Adding aluminum scrap recycling waste to the composition of the tested alkali activated materials (AAM) contributed to the porous structure of the material with the pore size ranging from 1,000 to 5,000 μm (detected by Micro-XCT, SEM). Lightweight (350–850 kg/m^3) and heat-resistant (up to 1,000°C) AAM with compressive strength from 1.0 to 3.0 MPa was obtained. The mineralogical composition of the obtained AAM was detected (XRD) and the heat resistant minerals in the structure of AAM were identified. It was concluded that the increased amount of Al_2O_3 in the raw material composition resulted in improved thermal stability of the AAM. In case where $\text{SiO}_2/\text{Al}_2\text{O}_3$ ratio is <2 , the formation of high-temperature resistant minerals, such as carnegite and nepheline, was observed. The obtained AAM could resist up to 8 thermal shock cycles and it could be easily adapted to the industrial production and application such as thermal insulation layer in laboratory furnaces.

Keywords: alkali activated material, porous materials, heat resistance, application in high temperature, aluminum scrap recycling waste

HIGHLIGHTS

- For the first time alkali activated materials were created on the chamotte-like and firebricks sawing residue precursors.
- Highly porous (up to 80 vol.%) structure of alkali activated materials were obtained by aluminum scrap recycling waste.
- For the first time the porous alkali activated materials was evaluated for high temperature application.
- The porous alkali activated materials manufacture is simple, sustainable, and based on mostly waste stream materials.
- Firebrick waste increased the temperature cycling performance of the material and proved to be highly suitable for industrial application.

INTRODUCTION

Low calcium alkali activated materials (AAM) or “Geopolymers” in some cases are the terms used to describe aluminosilicate-based inorganic polymers produced by mixing pozzolanic compounds or aluminosilicate source precursors and highly alkaline solutions (Davidovits, 1991). Production of AAM provide an opportunity to convert a variety of waste stream materials and by-products into useful, high value materials (Singh et al., 2015). Many factors can contribute to the alkali activation reaction mechanism and the properties of the final products, including (but not limited to) the aluminosilicate source precursors (Bumanis et al., 2017), the type of activator solution (Criado et al., 2007), the calcium content in the raw material mixture composition (Canfield et al., 2014), and the mixing and curing conditions (Moukannaa et al., 2018) as well as pore forming process (Bajare et al., 2014; Strozi et al., 2014; Seabra et al., 2016). AAM have attracted an increasing interest as fireproof materials associated with circular economy, namely, their production have low energy requirements and the final product is characterized by good mechanical performance, thermal behavior, and durability (Rashad et al., 2016). The existing publications on fire resistance and performance of AAM under high temperature conditions are promising.

The stability at high temperatures of binders made by the alkaline activation of aluminosilicate precursors is clearly distinct from the behavior observed in Portland cement at high temperatures (Martin et al., 2015). The shrinkage of AAM up to 600°C temperature occurs due to evaporation of the adsorbed and weakly bound water. Several reports indicate that the strength of AAM increases by the treatment at temperature between 600 and 800°C as densification occurs on the contrary with Portland cement-based materials (Fernández-Jiménez et al., 2010). In many cases melting process of AMM starts up to the temperature of 1,100°C (Kim and Kim, 2017). The resistance to high temperatures of AAM strongly depends from the composition of raw materials, i.e., Dupuy et al. has reported that all argillite-based AAM samples show low resistance to thermal shock (800°C, 10 min) and strength decreased up to 10 times (Dupuy et al., 2018), while other report by K. Hemra and P. Aungkavattana states that thermal shock resistance of metakaolin-based AAM at temperature of 800°C could reach up to 15 cycles (Hemra and Aungkavattana, 2016). In comparison with traditional refractory brick performance these results seems promising as their thermal shock resistance varies from 10 to 30 cycles (Philip, 2014).

One of the basic approaches to improve thermal properties of the AAM is to use fillers based on refractory materials. Bernal et al. reported that thermal behavior of metakaolinbased AAM with ground refractory brick filler (10–15 vol.%) could reduce the volumetric contraction and increase the residual compressive strength up to three times after exposure to high temperature in comparison with the AAM without fillers (Bernal et al., 2012).

Type and concentration of alkali activation solution play a dual role which calls for a certain compromise in the AAM design. On one hand, high alkali content in activation solution (8 to 12 M NaOH solutions) is necessary to accelerate the

activation reactions of precursors and to obtain AAM with high initial strength, but at the same time increased concentration of alkalis could act as fluxes at high temperatures. Therefore, the content of alkalis in the alkali activation solution must be limited to generate thermally stable materials (Martin et al., 2015). It has been reported that the alkali concentration in the activation solution could be reduced event to 2 M (Huiskes et al., 2016). The results of previous research show that increasing the SiO₂/Na₂O molar ratio of the activation solution the setting time of AAM mixture could also increase (Tchakoute et al., 2013). It has been reported that in cases, when ratio of SiO₂/Na₂O of activation solution is beyond optimum (>3.0), physical properties of the AAM can draw down quickly—water absorption increases while the bulk density does not change (Lemougna et al., 2011).

The aim of the present study is to assess the thermal stability of chamotte-like precursor based AAM with refractory brick by-product additive in order to achieve high mechanical properties after heat treatment and thermal shock resistance of the obtained material. The study includes development and demonstration of AAM production and application methods.

MATERIALS AND METHODS

Raw Materials

Commercially produced chamotte-like precursor (CH), where 36.9% of particles were with size lower than 45 μm was used in the research (Keramserwiss Ltd). According to the XRD analysis CH contains the following minerals: cristobalite (SiO₂), quartz (SiO₂), and mullite (Al₆Si₂O₁₃). Also minor amorphous phase as background hump was identified (**Figure 1**).

Firebrick sawing residues (K26) (Morgan Thermal Ceramics Ltd.) is classified as a by-product from the sawing process of insulation material typically used for furnace production. The K26 is aluminosilicate material and its chemical composition is given in **Table 1**. K26 was ground for 30 min by using planetary ball mill Retsch PM 400. 96.3% of the particles were with the size lower than 45 μm. According to the technical data sheet, working temperatures of the K26 range from 1,260 to 1,790°C. The K26 is made from high-purity refractory clay with high amount of Al₂O₃ (up to 60%). According to the XRD analysis, mullite (Al₆Si₂O₁₃) and corundum (Al₂O₃) as well as small background hump indicating amorphous phase were identified (**Figure 1**). K26 was considered as additional aluminum silicate source and as filling material which could improve thermal stability of the AAM.

Aluminum scrap recycling waste (ASRW) was received from the aluminum scrap recycling facility (Dilers Ltd). ASRW is the final waste, which is obtained from black dross in aluminum recovery process. ASRW was ground for 30 min by using planetary ball mill Retsch PM 400. Chemical composition of ASRW is given in **Table 1**; main oxides are Al₂O₃ (63.2 wt.%), SiO₂ (7.9 wt.%), CaO (2.6 wt.%), and Na₂O+ K₂O (7.7 wt.%). According to the XRD analysis, the ASRW contains quartz (SiO₂), spinel (MgAl₂O₄), iron (III) oxide (Fe₂O₃), calcium iron aluminum oxide (CaAlFe₄O₁₀), magnesium aluminum silicate (Mg₂Al₂Si₃O₁₂), aluminum iron oxide (FeAlO₃), and gibbsite (Al(OH)₃) (**Figure 1**). Ground ASRW with fraction <1 mm was

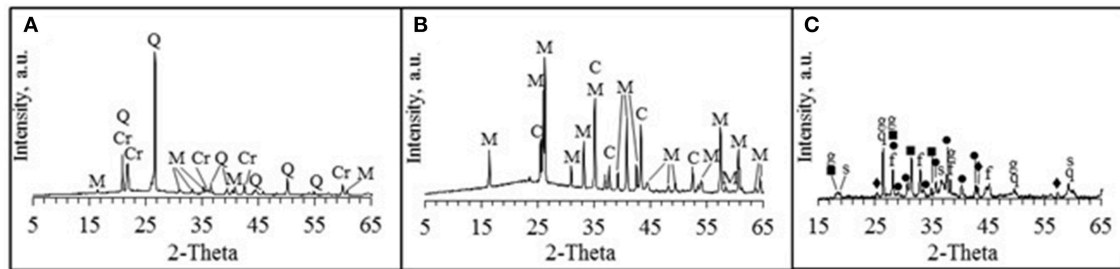


FIGURE 1 | X-ray analysis of solid raw materials, **(A)** CH, **(B)** K26, **(C)** ASRW; Q / q, quartz (85-0798 / 83-2187); Cr, cristobalite (03-0267); M, mullite (01-0613); C, corundum (71-1124); s, spinel (75-1799); f, iron oxide (32-0469); ■, calcium aluminum iron oxide (21-0830); ◆, magnesium aluminum silicate (30-0788); ●, aluminum iron oxide (18-0633); g, gibbsite (70-2038).

TABLE 1 | Chemical composition of solid raw materials, (weight %).

Raw materials	Al ₂ O ₃	SiO ₂	CaO	SO ₃	TiO ₂	MgO	Fe ₂ O ₃	Na ₂ O	K ₂ O	Other	LOI, 1,000°C
CH	18.8	76.7	0.3	0.0	1.2	0.5	0.7	1.0	0.8	0.3	0.00
K26	58.0	39.1	0.1	0.0	0.1	0.2	0.7	0.8	0.9	0.1	0.00
ASRW	63.2	7.9	2.6	0.4	0.5	4.4	4.5	3.8	3.8	2.6	6.21

TABLE 2 | Compositions of studied samples and amount of main oxides in pastes.

Composition	Mixture design, mass part				Main oxides in pastes, mass %			SiO ₂ / Al ₂ O ₃	SiO ₂ / Na ₂ O	Al ₂ O ₃ / Na ₂ O
	ASRW	CH	K26	6M NaOH	SiO ₂	Al ₂ O ₃	Na ₂ O			
Ref	0.10	1.00	0.00	0.36	53.08	17.21	3.41	3.1	11.1	5.0
0.1FB	0.10	0.90	0.10	0.36	50.50	19.89	3.40	2.5	10.6	5.9
0.3FB	0.10	0.70	0.30	0.36	45.35	25.26	3.37	1.8	9.6	7.5
0.5FB	0.10	0.50	0.50	0.36	40.20	30.63	3.34	1.3	8.6	9.2

used as the pore forming agent due to gas emissions, when it reacts with an activation solution (Bajare et al., 2012).

6 M NaOH solution, which was prepared by using sodium hydroxide flakes with 99% purity (Tianye Chemicals Ltd., China), was used as alkali activating solution.

Mixture Design and Sample Preparation

The basic AAM mixture compositions consisted of CH and ASRW with the mass ratio of 10:1. The mass ratio of the alkali activation solution to total solid raw materials ratio was 0.33. CH was partially substituted with sawing residues K26 up to 50 wt.% (Table 2). The theoretically calculated oxide ratios by mass are given in Table 2. The SiO₂ / Al₂O₃ ratio for studied AAM is in the range from 1.3 to 3.1, SiO₂ / Na₂O ratio—from 8.6 to 11.1 and Al₂O₃ / Na₂O—5.0 to 9.2. According to the report of Peigang He, the increased ratio of SiO₂/Al₂O₃ can increase mechanical properties of the AAM due to the increased amount of Si-O-Si bonds, which could appear in the polymerization process and presence of residual silica, which can operate as reinforcement (He et al., 2016). The decrease of Na₂O/Al₂O₃ ratio could cause less dissolution of precursors due to lower content of NaOH resulting in weaker active alkali activation reaction (Siyal et al., 2016).

The solid raw materials were mixed together and activation solution was added. After mixing with electrical twin shaft mixer for 2 min, the paste was immediately poured into prismatic molds (40 × 40 × 160 mm) sealed with plastic film and after formation of porous structure molds were covered and samples were cured at 80°C for 24 h. For thermal conductivity test and industrial application AAM plates of 45 × 45 × 5 cm were prepared. To characterize the effect of heat treatment on AAM properties prepared samples were treated at 800 and 1,000°C temperatures with the heating rate of 10°C/min and kept for 3 h at the max temperature. Three series of samples were prepared: Ref, 0.1FB, 0.3FB, and 0.5FB without heat treatment (i), Ref-800, 0.1FB-800, 0.3FB-800, and 0.5FB-800 with heat treatment at temperature 800°C (ii) and Ref-1000, 0.1FB-1000, 0.3FB-1000, and 0.5FB-1000 with heat treatment at temperature 1,000°C (iii). The obtained AAM samples were kept at ambient temperature (20 ± 2°C) for further testing.

Techniques

Chemical composition of the raw materials was determined according to LVS EN 196-2 with sensibility ±0.5 wt.%. The elemental analysis of ASRW was carried out with inductively coupled plasma optical emission spectrometry (ICP-OES) for Al

and Si, atomic absorption spectrometry (AAS) for Na, Mg, K, Ca, Fe, Cu, Zn, Pb. Potentiometer titration analysis (PTA) was used to determine Cl and combustion process—to determine S.

Thermogravimetric-differential thermal analysis (DTA/TG) was carried out by using Netzsch STA 409 PC from 0 to 1,200°C with the heating rate of 10°C/min. High temperature microscopy (HTOM) EM201, HT163 was used to determinate heat resistance and shrinkage of the AAM in temperatures up to 1,400°C. Samples were tested by heating rate 80°C/min up to 500°C temperature and then switched to 15°C/min, while reaching 1,400°C temperature.

The material density of AAM was measured by the geometric method using 40 × 40 × 40 mm specimens. The Archimedes principle (using water as immersion fluid) was employed to evaluate the specimens' water absorption, and combined with geometric measurements to determine the open porosity. The true density was determined for powdered AAM by using Le Chatelier flask and then the total porosity was calculated. X-ray computed tomography (XCT, Xradia μ CT-400, XRadia, Concord, USA with Avizo Fire 3D software) was employed to obtain 3D images of the AAM. Pore structure and porosity were assessed by using the XCT data and comparing the results to the traditional methods.

The AAM macro and microstructure was observed by using optical microscope and scanning electron microscope ("TESCAN Mira / LMU Field-Emission-Gun"). The thermal conductivity was measured with heat flow meter instrument LaserComp FOX 660.

Flexural and compressive strength of the prepared AAM samples 9 aged 28 days) were tested according to the LVS EN 196-1.

To determine the mineralogical composition of solid raw materials and AAM before and after heat treatment the X-ray diffraction (XRD) patterns of the powdered samples were recorded on a "RIGAKU ULTIMA+" diffractometer using CuK α radiation, the test was run in a 2-Theta range of 5–70° step-scan and 10 s/step.

The thermal cycling of the prismatic samples 40 × 40 × 160 mm was conducted in accordance with testing of refractory concrete (GOST 20910-90 Refractory concretes, 1991). The samples were kept for 60 min in a furnace heated to 800°C, then the samples were cooled for 20 min by a stream of air from a fan (700 W, 1,000 rpm). After each thermal cycle the speed of an ultrasonic pulse (SUSP) in the samples was determined and its decrease with respect to the SUSP values after heat treatment at 800°C was determined (Antonovich et al., 2011).

RESULTS

Thermal Analysis

DTA/TG

The changes of AAM during heat treatment up to 1,200°C could be described in four distinct phases (**Figure 2**). The first phase consists of evaporation of physically adsorbed water from the material matrix. Exothermic effect is appearing in DTA curve before heating temperature rises to 100–150°C (Djobo et al., 2016). The second phase begins at 150°C and

proceeds up to 600°C involving evaporation of the chemically bound water. It comes from dissolution of aluminosilicate raw materials, when aluminate and silicate species are formed. In this phase significant processes contributing to the knowledge base about the extent of alkali activation reaction can be observed (Firdous et al., 2018). Namely, the TGA result showed similar behavior of AAM, when between 150 and 600°C the mass loss was 2.91 and 2.67% respectively. The mass loss ~5% in the temperature between 500 and 700°C as well as start of another mass loss region at 900°C along with minor features on the differential scanning calorimeter represented various phases of crystallization (Canfield et al., 2014). The densification of AAM occurs at 820–920°C. Onset temperatures decrease slightly and sharply appear due to softening and viscous sintering (Barbosa and MacKenzie, 2003; Villaquirán-Caicedo et al., 2017). Another minor weight loss of 0.4% at the temperature around 800°C is associated with the decomposition of calcite which in minor parts was detected in ASRW. Finally, rapid densification and weight loss was observed above 1,000°C.

High Temperature Microscopy (HTOM)

HTOM results can be divided in three relative intervals which correlate well with DTA/TG results: (a) specific area changes at the temperature up to 800°C; (b) from 800 to 1,000°C; and (c) from 1,000 to 1,200°C (**Figure 3**; **Table 3**). Shrinkage of the AAM with the intensity from 3.2 to 4.9% was observed at the temperature up to 1,000°C.

Physical and Mechanical Properties

The physical properties of the porous AAM are given in **Figure 4**. The density of porous AAM was in the range from 670 to 755 kg/m³. The total porosity of the obtained materials was between 71 and 75 vol.%. The open porosity was from 27 to 30 vol.%. The pore structure of the obtained materials remain open which corresponds to the water absorption. The water absorption of the AAM was between 45 and 48 wt.%.

The thermal conductivity of prepared porous AAM plates (45 × 45 × 5 cm) was measured. The measured thermal conductivity was from 0.14 to 0.15 W/m·K and it was not affected by the mixture composition of AAM but correlated well with total porosity of the material.

The porosity measured by the micro-XCT indicated the total pore value ranging from 41.2 to 52.7 vol.% with the pore structure of the AAM, pore distribution as well as the measurement technique being the factors contributing to these differences. Three-dimensional internal pore structure of the specimens was made and pore size distribution was reconstructed using 3D-image analysis software (Avizo Fire) (**Table 4**). According to the research results the size of most of the pores in the material (90.2 vol.%) was between 1,000 and 5,000 μ m. It can be clearly seen in the pore sieving images obtained by using the Avizo Fire 3D software. The pores within the range from 7E+9 to 9E+9 μ m³ have a blue color, whereas the pores having a size greater than 9E+9 μ m³ have a green color (**Figure 5**).

The compressive and flexural strength results of the AAM are presented in **Figure 6**. The compressive strength was 1.1 MPa for Ref and increased to 2.0 MPa for 0.5FB. After sample

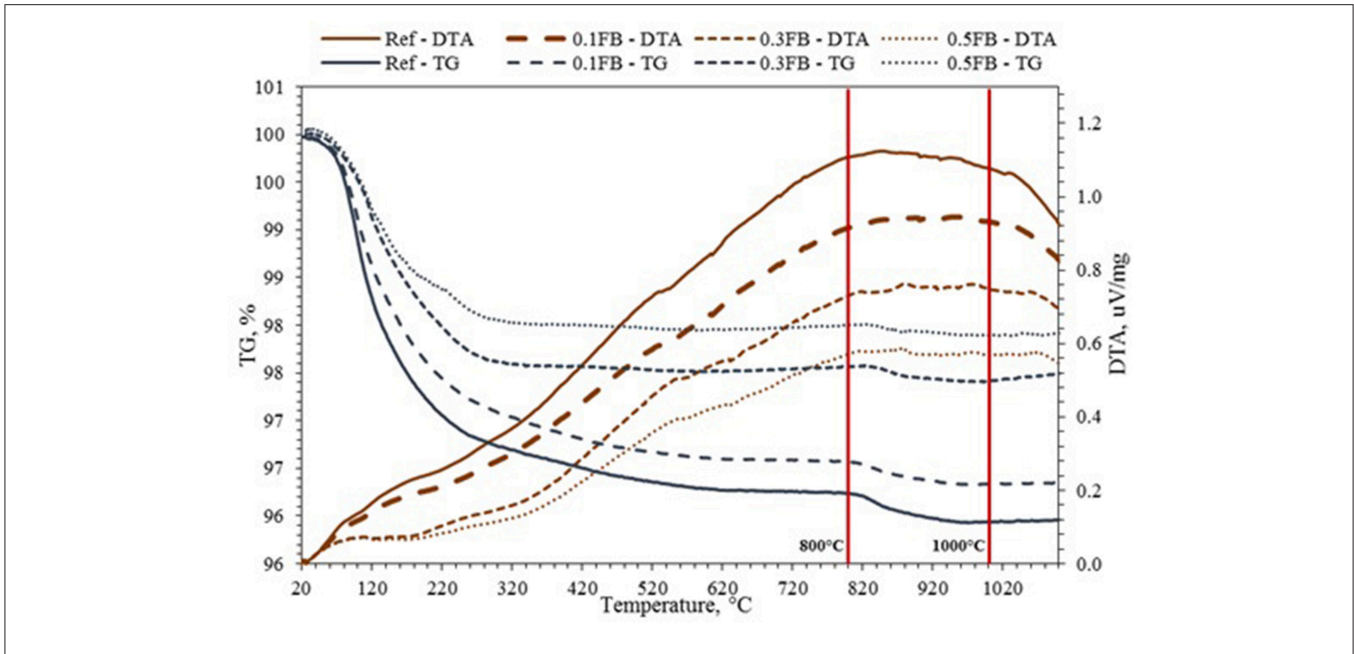


FIGURE 2 | DTA /TG curves for the porous AAM.

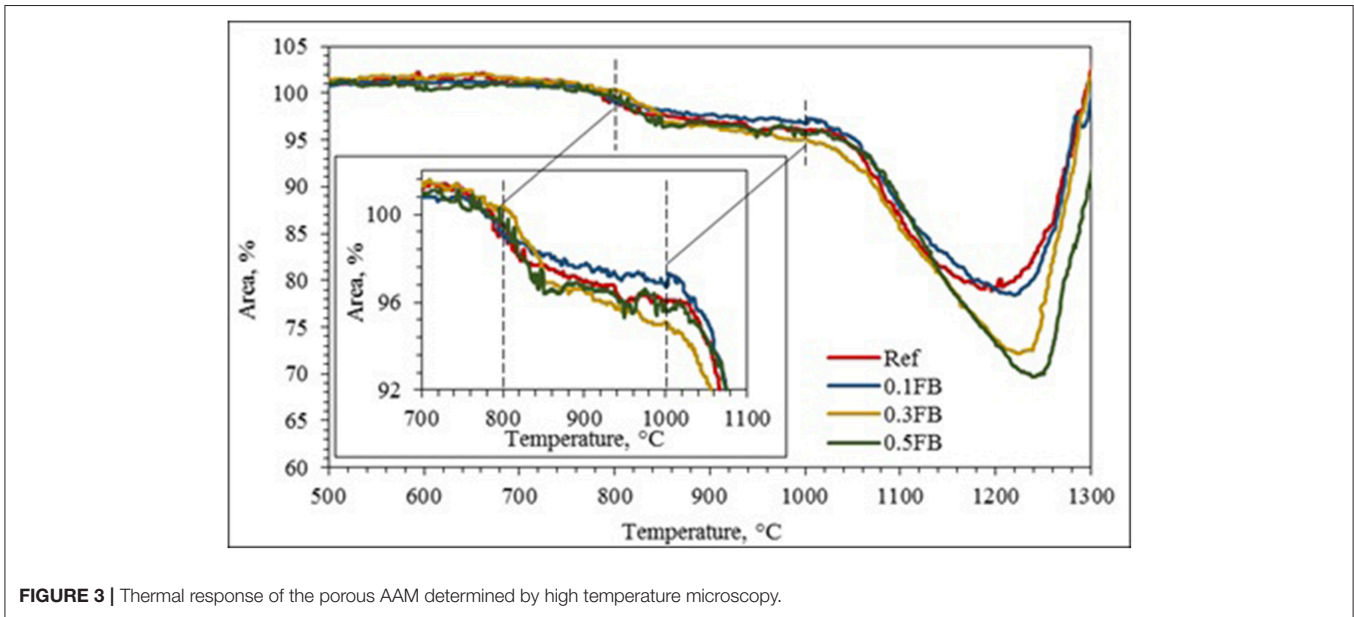


FIGURE 3 | Thermal response of the porous AAM determined by high temperature microscopy.

TABLE 3 | Relative area changes of obtained porous AAM.

Composition	Temperature/shrinkage		Shrinkage/temperature			
	800°C	1,000°C	5%	10%	15%	20%
Ref	0.5%	4.0%	1,042°C	1,080°C	1,109°C	1,165°C
0.1FB	1.0%	3.2%	1,052°C	1,087°C	1,124°C	1,177°C
0.3FB	-0.4%	4.9%	984°C	1,073°C	1,104°C	1,148°C
0.5FB	0.5%	4.3%	1,036°C	1,091°C	1,118°C	1,146°C

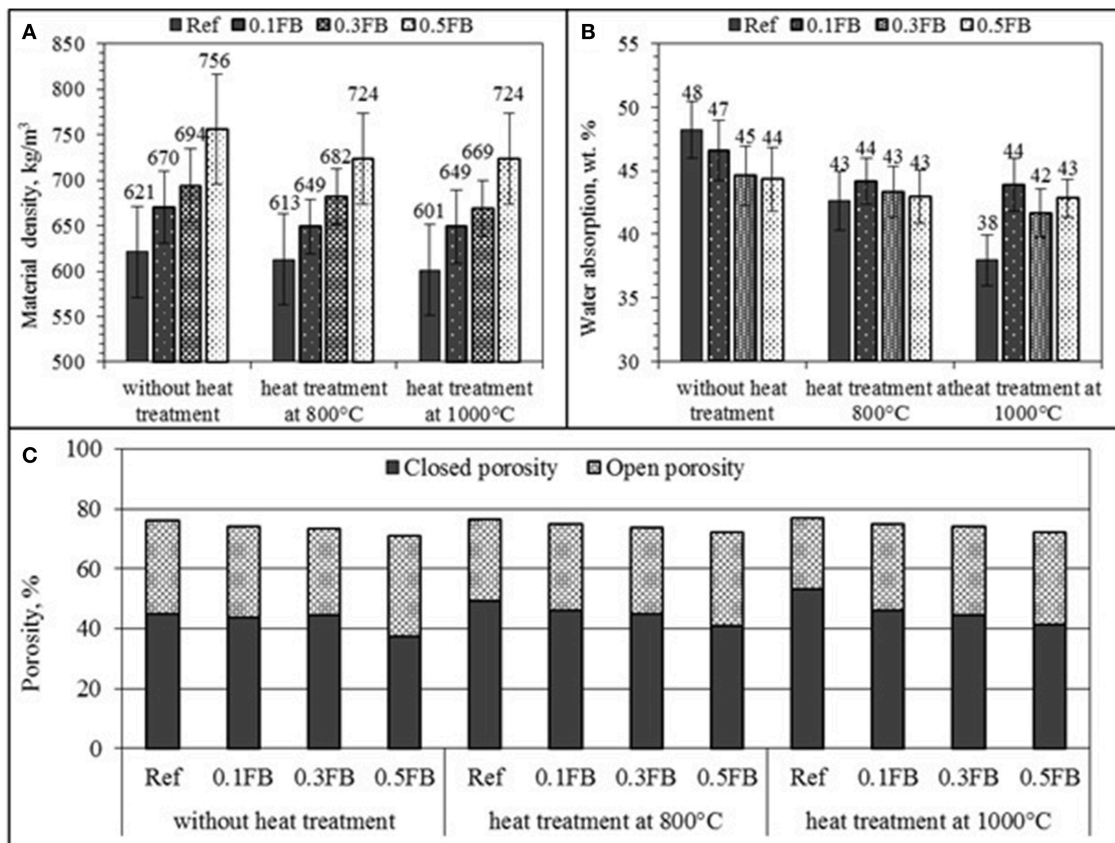


FIGURE 4 | The physical properties of porous AAM, **(A)** material density, **(B)** water absorption, **(C)** porosity.

TABLE 4 | Volumetric pore size distribution (vol. %) of 0.5FB determined by Micro-XCT.

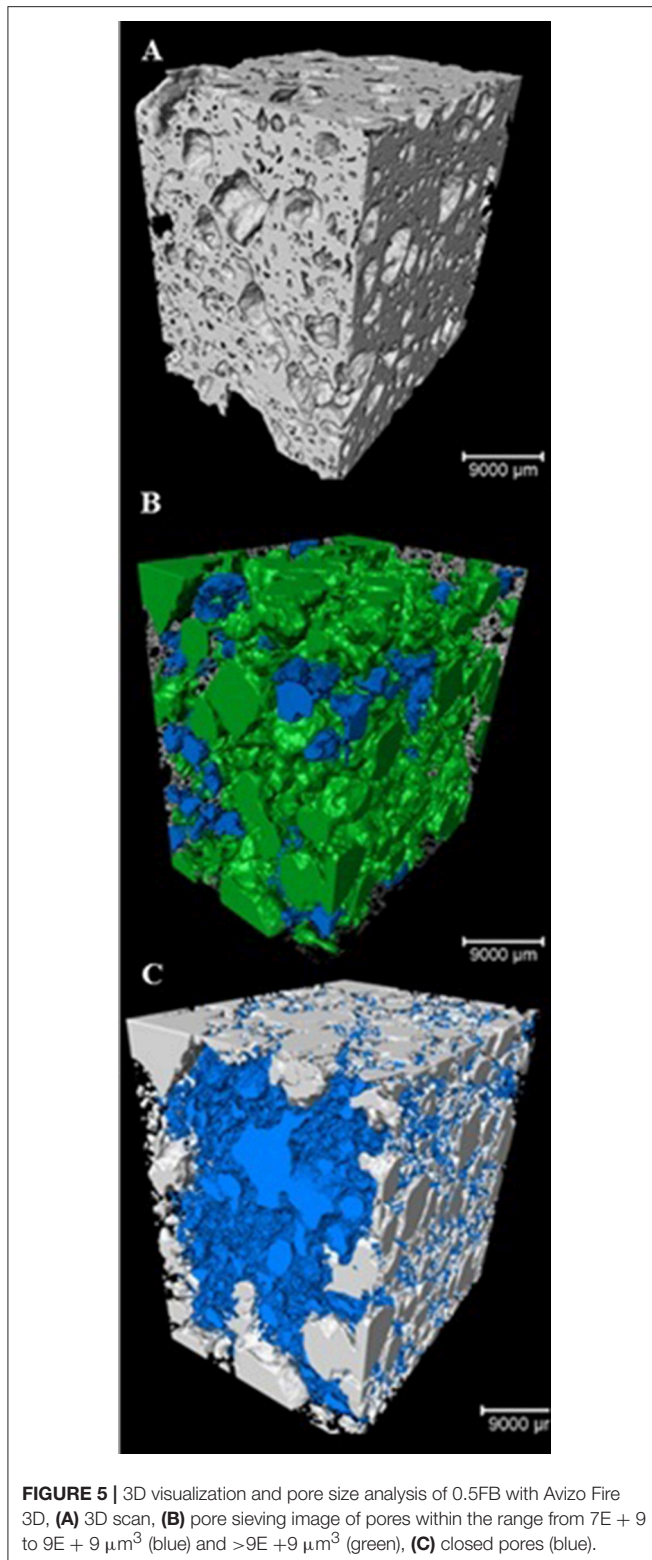
≤100 μm	100–250 μm	250–500 μm	500–1,000 μm	1,000–5,000 μm	≥5,000 μm
0.0	0.5	1.9	4.3	90.2	3.1

treatment at 800°C, compressive strength was 0.7 for Ref and 0.9 MPa for 0.1FB. Slight strength increase was for 0.3FB, while for the 0.5FB strength increased to 2.5 MPa. The heat treatment at 1,000°C slightly increased strength comparing to samples treated at 800°C for the mixture compositions Ref, 0.1FB and 0.3FB. The composition 0.5FB had compressive strength 2.7 MPa.

The flexural strength for all samples except for 0.5FB before heat treatment was in a range from 0.5 to 0.6 MPa, while the strength of 0.5FB samples was 0.8 MPa. The flexural strength decreased to 0.3–0.5 MPa for samples with Ref, 0.1FB, 0.3FB but the increase of flexural strength was observed for 0.5FB—reaching 1.0 MPa. Similar tendency was observed for the heat treated samples at 1,000°C. Structural integrity was preserved and insignificant or no strength loss was observed compared with specimens treated at 800°C temperature.

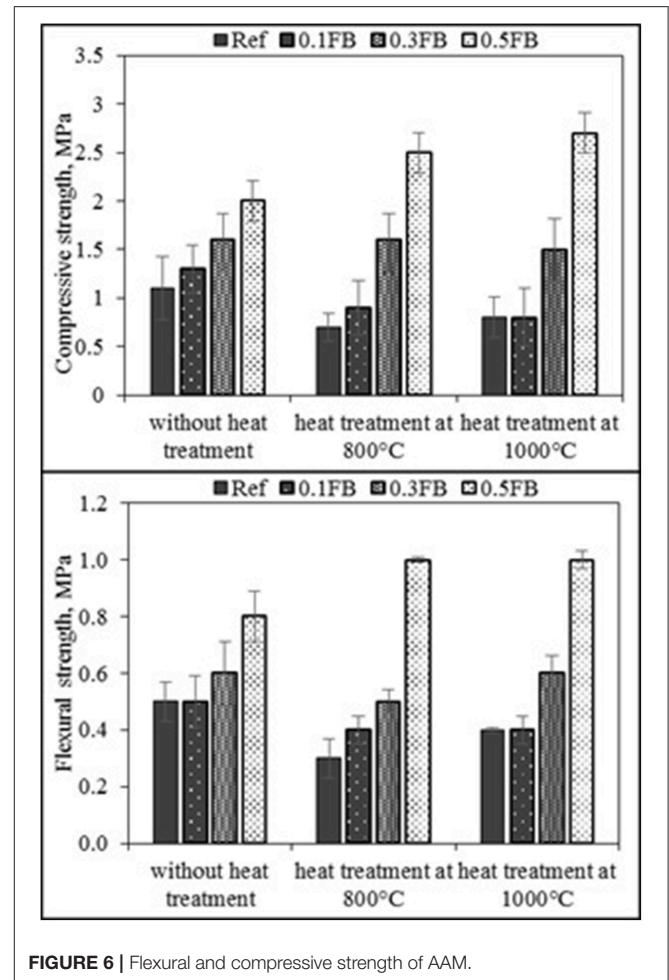
X-Ray Diffraction

The XRD was determined for blends of solid raw material (Figure 7 with index raw), prepared porous AAM before and after heat treatment at 800 and 1,000°C for mixture compositions Ref and 0.5FB. After alkali activation slight phase change was observed for Ref but almost all minerals detected in mix of raw materials were still present in the AAM. The composition Ref had crystalline phases, which have remained from precursors (CH) like mullite ($\text{Al}_{4.56}\text{Si}_{1.44}\text{O}_{9.72}$), quartz (SiO_2), and cristobalite (SiO_2). After alkali activation low intensity peaks of analcime appeared, but after heat treatment at 800 and 1,000°C crystalline phase of analcime disappeared and new crystalline phases have not been detected. Meanwhile composition 0.5FB had crystalline phases, which had remained from precursors like mullite ($\text{Al}_{4.56}\text{Si}_{1.44}\text{O}_{9.72}$), quartz (SiO_2), corundum (Al_2O_3), and cristobalite (SiO_2). Hydroxy sodalite ($1.08\text{Na}_2\text{O} \cdot \text{Al}_2\text{O}_3 \cdot 1.68\text{SiO}_2 \cdot 1.8\text{H}_2\text{O}$; sodalite group zeolites) and N-A-S-H gel which are formed during the activation process were also detected. The hydroxy sodalite was not detected after heat treatment of specimens at 800°C temperature, but new crystalline phase carnegite (NaAlSiO_4) was present. After heat treatment at 1,000°C phases such as quartz, mullite, corundum, and cristobalite remained, but new crystalline phase—nepheline ($\text{Na}_{6.65}\text{Al}_{6.24}\text{Si}_{9.76}\text{O}_{32}$) was detected.



Cycling Performance

The cyclic performance of the prepared AAM was evaluated (**Figure 8**). Pre-treatment of separate batch of samples was done to reduce first thermal shock induced by the formation



of new minerals inside the AAM previously detected by the XRD. The ultrasonic pulse velocity was measured to evaluate the performance. The cycling results are given in **Table 5**. The first thermal cycle at the temperature of 800°C reduced the initial ultrasonic pulse velocity by 30 to 50%, while the critical value of 300 m/s was not reached. The 2nd high temperature cycle was crucial for the samples Ref, Ref_800 and 0.1FB with the ultrasonic pulse velocity decrease below 300 m/s. With the increasing proportion of K26 in the mixture composition of AAM the thermal cycle performance improved and up to 7 cycles were achieved for the specimens 0.5FB_800.

DISCUSSION

The mass loss intensity during TGA analysis can be used to measure the extent of alkali activation (**Figure 2**). Higher overall mass loss relates to higher extent of alkali activation as more water is attracted to hydrated NASH gel (Vogt et al., 2016). Increased weight loss was observed for 0.5FB as higher amount of K26 filler was incorporated in the mixture composition of AAM, showing the positive role of K26 in alkali activation process.

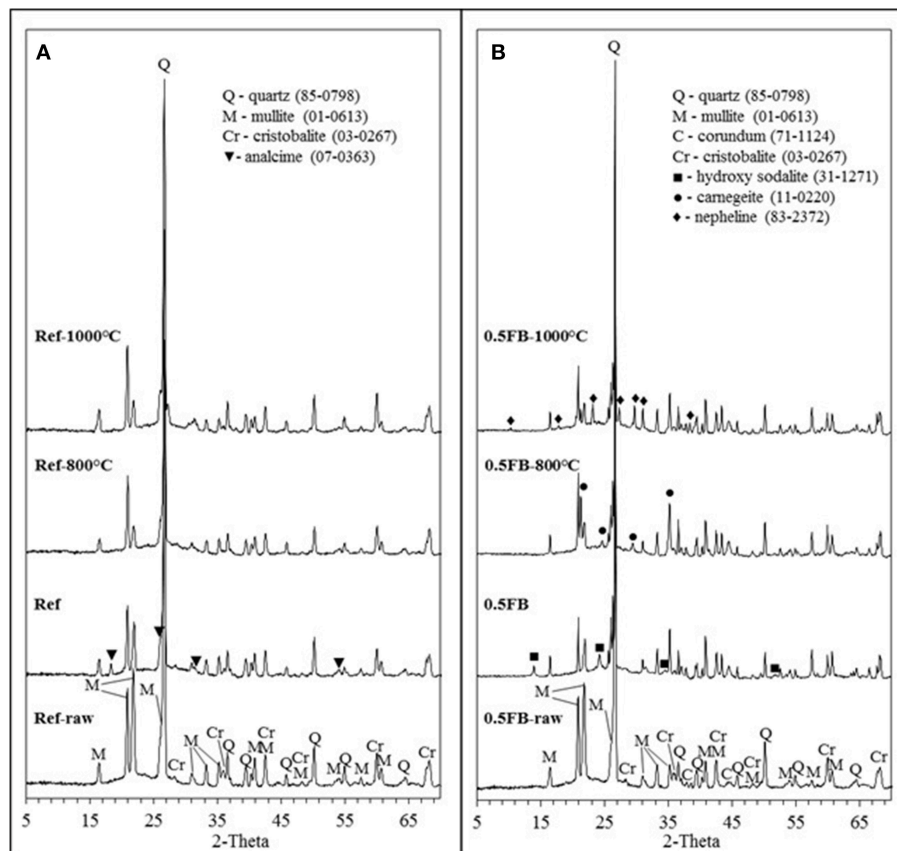


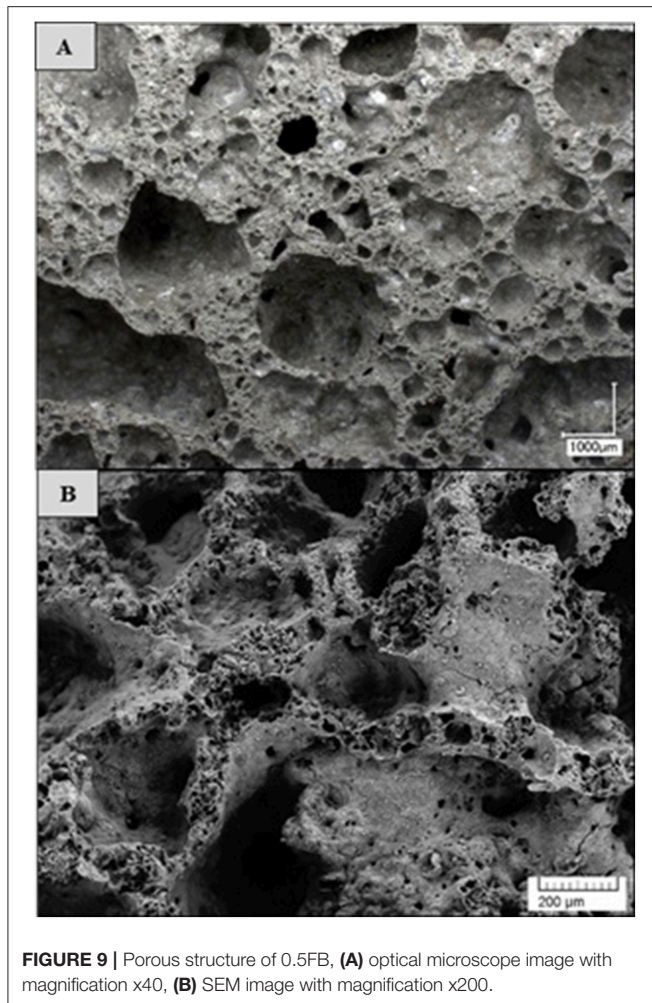
FIGURE 7 | XRD analysis of obtained porous AAM and solid raw material mixtures, **(A)** porous AAM based on chamotte-like clay (Ref), **(B)** porous AAM based on chamotte-like clay and firebricks sawing residues (0.5FB).



FIGURE 8 | High temperature cyclic performance of AAM. Heating and cooling cycle.

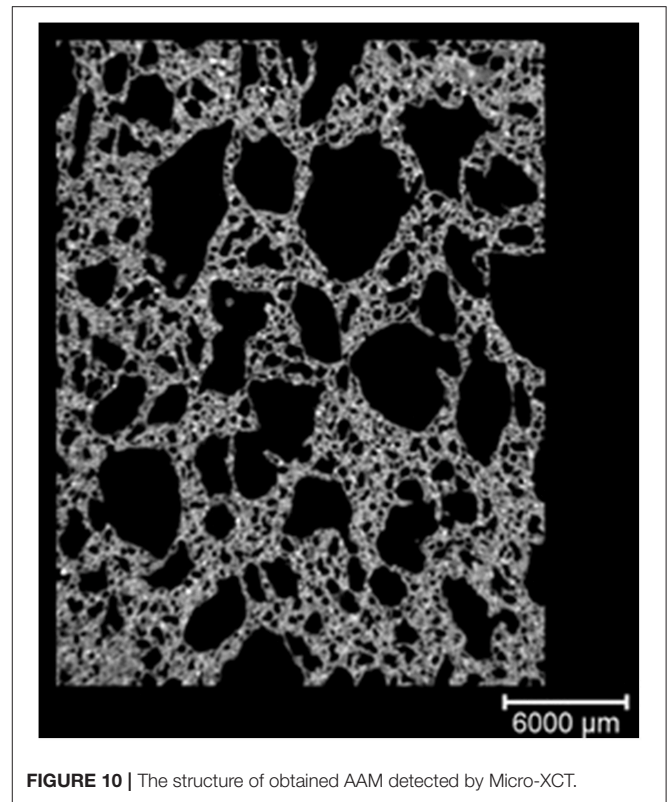
The DTA/TG results showed that at the interval between 800 and 1,000°C the structural changes could take place; therefore, further investigation was done at selected temperatures. Since the DTA/TG results showed similar performance between Ref up to 0.5FB with different K26 concentration in mixture composition, for the ease of result interpretation compositions Ref and 0.5FB were compared except in cases, where noticeable differences were detected.

Thermal expansion can be limited by highly porous structure of the AAM (**Figure 3**). The deformations in specimen can take place inside the pores and true expansion value could be even greater. Some expansion was attributed to the transformation of α -quartz to the β -quartz which follows the volume increase of specimens at the temperature 573°C. Due to transformation of quartz and expansion of specimens the microstructure of AAM could be damaged, which could have negative influence on the



mechanical properties. According to the literature the second interval from 800 to 1,000°C is associated with melting of alkalis. At temperatures over 800°C solid raw materials are attacked by alkalis, which causes partial sintering in the contact zone between the geopolymer matrix and the aggregate, which in this case is unreacted crystalline phases remained from raw materials. This effect plays a substantial role in the improvement of residual mechanical properties after exposure to 1,000°C and helps AAM to resist higher temperatures without damage (Mandal et al., 2011; Rovnaník and Šafránková, 2016).

The physical and mechanical properties were slightly affected by the selected mixture compositions. Porosity within the material structure, as well as the material density, depends on the gas supply in the fresh paste. The chemical reaction between the ASRW and the alkali solution as well as generated heat flux leads to gas formation in the fresh paste. Low viscosity of the fresh paste and the pressure of evolved gasses in the process of pore formation are the factors, which cause breaking down of the walls and coalescence of pores, thus small bubbles diffuse into the bubbles, which are larger (Figures 9, 10). The above mentioned observations show the differences between the pore formation using ASRW as pore formation agent and other possible solutions



such as H₂O₂ (Ducman and Korat, 2016). Structure formation, gas release, and the evaporation of free water during initial setting of AAM are the factors contributing to high open porosity (up to 33%). In the SEM microphotographs it is possible to observe micropores not exceeding few micrometers (Figure 9B). As these small micropores were not detected by the Avizo Fire 3D software due to insufficient resolution of X-ray computed tomography, it is possible that some of the pores are not included in the calculations of porosity by the micro-XCT (Dembovska et al., 2017). The results of the pore analysis obtained using Avizo Fire 3D software include only the pores being larger than 48 μm (identified as macropores), whereas the difference between the total porosity detected by using the Le Chatelier flask and the porosity detected by the Avizo Fire 3D software show both micro and capillary pores.

The amount and structure of pores had influence on compressive strength of the AAM giving characteristically low compressive strength associated with highly porous materials. The increase of K26 amount in the composition of AAM increased the initial compressive strength. The heat treatment of samples at the temperature of 800°C reduced compressive strength for Ref and 0.1FB to 0.7 and 0.9 MPa, respectively, indicating strength reduction by 36 and 32% while for the 0.5FB strength increase was 24% reaching 2.5 MPa. The heat treatment at 1,000°C led to slight strength gain comparing to the samples treated at 800°C for the mixture compositions Ref, 0.1FB and 0.3FB, while it was still lower comparing to the samples without heat treatment. The composition 0.5FB had further strength increase up to 2.7 MPa (8% increase

TABLE 5 | Ultrasonic pulse velocity after high temperature cycling.

No of cycle	Ultrasonic pulse velocity, m/s							
	Ref	Ref_800	0.1FB	0.1FB_800	0.3FB	0.3FB_800	0.5FB	0.5FB_800
0	1661	889	1,682	898	1,590	1,084	1,520	1,433
1	681	480	794	574	831	737	1,365	1,101
2	160	213	262	379	515	466	1,100	705
3	139	236	218	158	411	325	787	624
4	–	139	144	161	266	325	763	625
5	–	–	–	–	178	384	569	572
6	–	–	–	–	171	384	482	593
7	–	–	–	–	153	175	306	317

Acceptable results has been highlighted green, i.e. values over 300.

comparing to the strength at 800°C) indicating the improved structure performance with the incorporation of higher proportion of K26.

The XRD results indicate the N-A-S-H gel formation during alkali activation process and it was detected by the shift of halo at 2-Theta = 10–30° to higher degrees (Zhang et al., 2012) in both cases (for Ref and 0.5FB before heat treatment respectively). The phase transformation was identified during heat treatment of AAM. It could be explained by transformation of initially detected hydroxide sodalite into zeolite X, which melts at 760°C temperature and becomes amorphous but later it recrystallizes again at 800°C and crystallizes as carnegite (Jacobs, 1984). After further temperature increase the nepheline transforms from the carnegite at the temperature around 900–1,000°C. Considerable change of the N-A-S-H gel after heat treatment at different temperatures was not detected by X-ray diffraction.

Also phase changes was detected by XRD and the first controlled pre-treatment at the temperature of 800°C was applied for porous AAM, it did not improve the overall cyclic performance of AAM and only initiated the early deterioration of AAM structure by showing possible relationship between pre-treatment and first cyclic load for untreated samples. Each additional cycle continued to damage structure of the AAM.

HIGH TEMPERATURE CYCLIC PERFORMANCE AND INDUSTRIAL APPLICATION

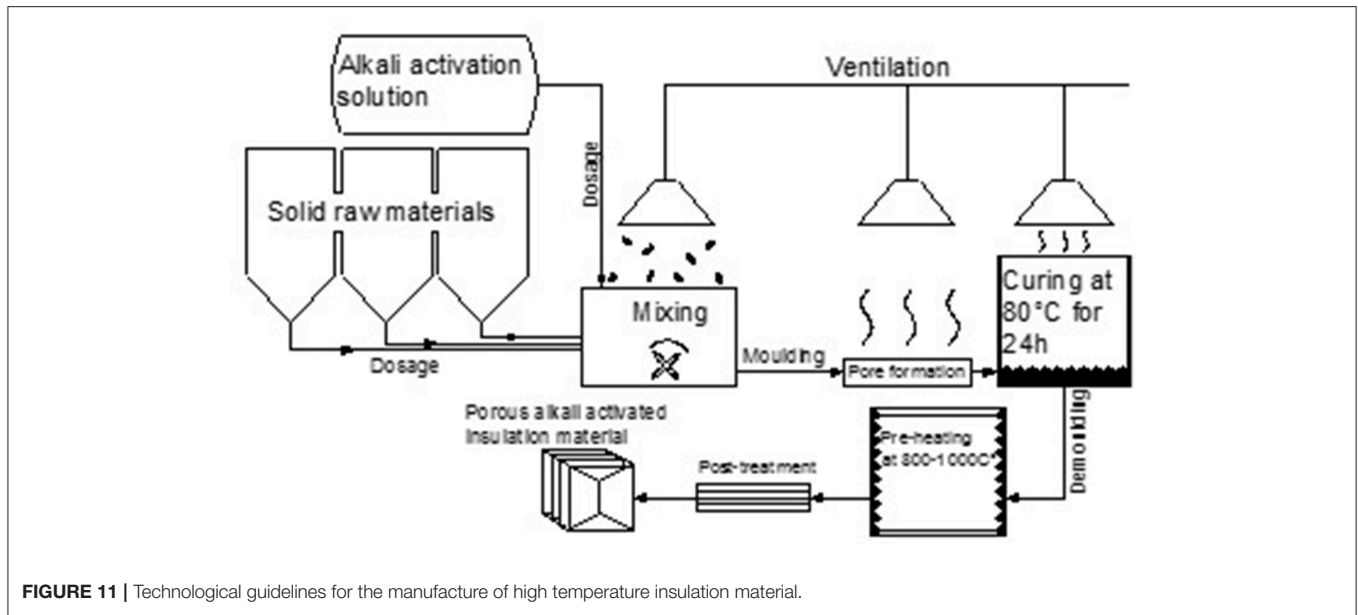
Technological Perspective of High Temperature AAM Production: Production Process

The schematic diagram of the AAM production process is given in Figure 11. The estimation of AAM mixture composition regarding raw material chemical composition should be calculated to cover the optimum range of main oxide ratios. The production process consists of dosage of raw materials and pre-mixing to obtain homogenous precursor for alkali activation. It should be noted that ASRW and K26

components must be pre-treated by milling to obtain fine, powder-like material. After adding alkali activation solution and mixing, paste should be molded instantly to allow blowing agent to react and form porous structure of the AAM. If prolonged mixing or molding time is necessary, the cooling process of raw materials should be considered (reaching –20°C) to delay the initial exothermic reaction provided by the ASRW, which determines rapid setting of the AAM. The further process control related to the curing regime should be maintained at 80°C for 24 h. The ventilation and filtering of gasses emitted by the ASRW during blowing of AAM should be ensured to provide safe production process and to avoid environmental pollution. After the AAM are demoulded, high temperature pre-treatment at 800°C could be applied to the allow phase change transformations take place to ensure further dimensional stability before cutting the material and creating final shape of the detail.

Technological Perspective of High Temperature AAM Production: Industrial Approbation

Following the previously described technological process, AAM plates for industrial application were prepared. 45 × 45 × 5 cm porous AAM plates were made in the laboratory conditions and provided to the producer of laboratory furnaces. During further processing of the prepared AAM plates they proved to be workable with traditional tools (Figure 12). The high temperature oven prototype was created by combining prepared porous AAM insulation plates with traditional refractory insulation materials. The prepared AAM was placed as outer insulation layer of the oven. The possible limitations of the AAM described is the relatively low strength of the material which is associated with high porosity; therefor the application of the material is suggested to be used as the interlayer material in high temperature furnaces which main function would be heat insulation. Other limitation which is related with production process is associated with the availability of the raw materials and its nature, as most of them are industrial wastes and by-products so the production of the material must be carefully controlled.



CONCLUSIONS

The investigated porous alkali activated material (AAM), which is based on chamotte-like precursor, firebrick sawing residues and aluminum scrap recycling waste, proved to be suitable for industrial production and applications.

The tested alkali activated material had high porosity (open porosity 25–30 vol.%, total porosity 71–75 vol.%), reasonable strength (before heat treatment from 1.1 to 2.1 MPa and after treatment at 1,000°C 0.8–2.6 MPa, respectively) and effective working temperature up to 800 (shrinkage from –0.4 to 1.0%) and 1,000°C (shrinkage from 3.2 to 4.9%).

High thermal stability of porous AAM reaching up to 8 thermal shock cycles was obtained. It is suggested that the ultrasonic pulse velocity lower limit of 300 m/s could be acceptable for non-destructive testing method for porous AAM, as samples withstand thermal cycling load and remain solid appearance and still reasonable strength.

The macropore (>48 μm) structure of AAM could be effectively determined by the X-ray computed tomography with Avizo Fire 3D software giving possibility to test structure with non-destructible method i.e., for quality control during the production. Though to characterize the total porosity test methods based on the Archimedes principle should be used.

The obtained material has a simple, reproducible and low-cost manufacture ensuring maximal valorization of waste into a heat-resistant material with high added value. The firebrick sawing residue incorporation in the composition of AAM improved the performance of heat resistance as the increase of Al₂O₃ content was achieved. This innovative waste-based material was treated at temperature 1,000°C and proved to be suitable for application at the temperature up to 1,000°C.

It was proved that the developed material is effective for industrial production and could be a promising for using as outer insulation layer in high temperature furnaces.

AUTHOR CONTRIBUTIONS

All co-authors are working together on porous AAM for different kind of applications since 2013. DB is the main author of this manuscript and supervisor of all other co-authors. LV is a Ph.D. student and her responsibility at this research was to analyze XRD

results, as well as other obtained data. LD is the last year Ph.D. student and this research is included in her thesis, so most of the tests have been done by LD. GB is leading researcher, as his Ph.D. thesis was about porous AAM and he has the experience of the work with aluminum scrap recycling waste usage in AAM production he was helping with data interpretation.

REFERENCES

- Antonovich, V., Shyukhta, M., Pundene, I., and Stonis, R. (2011). Procedural elements in estimation of the thermal shock resistance of different types of refractory concrete based on chamotte filler. *Refract. Ind. Ceram.* 52, 70–74. doi: 10.1007/s11148-011-9369-y
- Bajare, D., Bumanis, G., Korjakins, A., and Sele, L. (2014). Reuse of non-metallic residues from aluminium recycling industry in production of porous building materials. *Constr. Mater. Struct.* 1, 136–144. doi: 10.3233/978-1-61499-466-4-136
- Bajare, D., Korjakins, A., Kazjonovs, J., and Rozenstrauha, I. (2012). Pore structure of lightweight clay aggregate incorporate with non-metallic products coming from aluminium scrap recycling industry. *J. Eur. Ceram. Soc.* 32, 141–148. doi: 10.1016/j.jeurceramsoc.2011.07.039
- Barbosa, V. F. F., and MacKenzie, K. J. D. (2003). Thermal behaviour of inorganic geopolymers and composites derived from sodium polysialate. *Mater. Res. Bull.* 38, 319–331. doi: 10.1016/S0025-5408(02)01022-X
- Bernal, S. A., Bejarano, J., Garzón, C., Mejía De Gutiérrez, R., Delvasto, S., and Rodríguez, E. D. (2012). Performance of refractory aluminosilicate particle/fiber-reinforced geopolymer composites. *Compos. Part B Eng.* 43, 1919–1928. doi: 10.1016/j.compositesb.2012.02.027
- Bumanis, G., Vitola, L., Bajare, D., Dembovska, L., and Pundiene, I. (2017). Impact of reactive SiO₂/Al₂O₃ ratio in precursor on durability of porous alkali activated materials. *Ceram. Int.* 43, 5471–5477. doi: 10.1016/j.ceramint.2017.01.060
- Canfield, G. M., Eichler, J., Griffith, K., and Hearn, J. D. (2014). The role of calcium in blended fly ash geopolymers. *J. Mater. Sci.* 49, 5922–5933. doi: 10.1007/s10853-014-8307-z
- Criado, M., Fernández-Jiménez, A., and Palomo, A. (2007). Alkali activation of fly ash: effect of the SiO₂/Na₂O ratio. Part I: FTIR study. *Microporous Mesoporous Mater.* 106, 180–191. doi: 10.1016/j.micromeso.2007.02.055
- Davidovits, J. (1991). Geopolymers. *J. Therm. Anal.* 37, 1633–1656. doi: 10.1007/BF01912193
- Dembovska, L., Bajare, D., Ducman, V., Korat, L., and Bumanis, G. (2017). The use of different by-products in the production of lightweight alkali activated building materials. *Constr. Build. Mater.* 135, 315–322. doi: 10.1016/j.conbuildmat.2017.01.005
- Djubo, J. N. Y., Elimbi, A., Tchakouté, H. K., and Kumar, S. (2016). Reactivity of volcanic ash in alkaline medium, microstructural and strength characteristics of resulting geopolymers under different synthesis conditions. *J. Mater. Sci.* 51, 10301–10317. doi: 10.1007/s10853-016-0257-1
- Ducman, V., and Korat, L. (2016). Materials Characterization Characterization of geopolymer fly ash based foams obtained with the addition of Al powder or H₂O₂ as foaming agents. *Mater. Charact.* 113, 207–213. doi: 10.1016/j.matchar.2016.01.019
- Dupuy, C., Gharzouni, A., Sobrados, I., Texier-Mandoki, N., Bourbon, X., and Rossignol, S. (2018). Thermal resistance of argillite based alkali-activated materials. Part 2: identification of the formed crystalline phases. *Mater. Chem. Phys.* 218, 262–271. doi: 10.1016/j.materchemphys.2018.07.036
- Fernández-Jiménez, A., Pastor, J. Y., Martín, A., and Palomo, A. (2010). High-temperature resistance in alkali-activated cement. *J. Am. Ceram. Soc.* 93, 3411–3417. doi: 10.1111/j.1551-2916.2010.03887.x
- Firdous, R., Stephan, D., and Yankwa Djubo, J. N. (2018). Natural pozzolan based geopolymers : a review on mechanical, microstructural and durability characteristics. *Constr. Build. Mater.* 190, 1251–1263. doi: 10.1016/j.conbuildmat.2018.09.191
- GOST 20910-90 Refractory concretes (1991). *Specifications*. Available online at: <http://docs.cntd.ru/document/9052226> (accessed October 17, 2018).
- He, P., Wang, M., Fu, S., Jia, D., Yan, S., Yuan, J., et al. (2016). Effects of Si/Al ratio on the structure and properties of metakaolin based geopolymer. *Ceram. Int.* 42, 14416–14422. doi: 10.1016/J.CERAMINT.2016.06.033
- Hemra, K., and Aungkavattana, P. (2016). Effect of cordierite addition on compressive strength and thermal stability of metakaolin based geopolymer. *Adv. Powder Technol.* 27, 1021–1026. doi: 10.1016/J.APT.2016.04.019
- Huiskes, D.M. A., Keulen, A., Yu, Q. L., and Brouwers, H. J. H. (2016). Design and performance evaluation of ultra-lightweight geopolymer concrete. *Mater. Des.* 89, 516–526. doi: 10.1016/J.MATDES.2015.09.167
- Jacobs, P. A. (1984). “Structure and reactivity of modified zeolites,” in *Proceedings of an International Conference* (Prague: Elsevier). Available online at: <https://books.google.lv/books?id=lekhAQAQAQBAJ&pg=PA171&dq=%22carnegeite%22+zeolite&hl=en&sa=X&ved=0ahUKEwiC0prjndPTAhXiDZoKHb8fCmUQ6AEIJzAB#v=onepage&q=%22carnegeite%22zeolite&f=false> (accessed September 19, 2018).
- Kim, S., and Kim, Y. (2017). *Ceramic Processing Research Property Enhancement of Geopolymers After Heat Treatment*. Available online at: http://jcpr.kbs-lab.co.kr/file/JCPR_vol.18_2017/JCPR18-1/11.2016-182_59-63.pdf (accessed October 17, 2018).
- Lemougna, P. N., MacKenzie, K. J. D., and Melo, U. F. C. (2011). Synthesis and thermal properties of inorganic polymers (geopolymers) for structural and refractory applications from volcanic ash. *Ceram. Int.* 37, 3011–3018. doi: 10.1016/j.ceramint.2011.05.002
- Mandal, K. K., Thokchom, S., and Roy, M. (2011). Effect of Na₂O content on performance of fly ash geopolymers at elevated temperature. *Int. J. Environ. Chem. Ecol. Geophys. Eng.* 5, 7–13. doi: 10.5281/zenodo.1058857
- Martin, A., Pastor, J. Y., Palomo, A., and Fernández Jiménez, A. (2015). Mechanical behaviour at high temperature of alkali-activated aluminosilicates (geopolymers). *Constr. Build. Mater.* 93, 1188–1196. doi: 10.1016/J.CONBUILDMAT.2015.04.044
- Moukannaa, S., Loutou, M., Benzazoua, M., Vitola, L., Alami, J., and Hakkou, R. (2018). Recycling of phosphate mine tailings for the production of geopolymers. *J. Clean. Prod.* 185, 891–903. doi: 10.1016/j.jclepro.2018.03.094
- Philip, C. (2014). Performance evaluation of refractory bricks produced from locally sourced clay materials. *J. Appl. Sci. Environ. Manag.* 18, 151–157. doi: 10.4314/jasem.v18
- Rashad, A. M., Hassan, A. A., and Zeedan, S. R. (2016). An investigation on alkali-activated Egyptian metakaolin pastes blended with quartz powder subjected to elevated temperatures. *Appl. Clay Sci.* 132–133, 366–376. doi: 10.1016/J.CLAY.2016.07.002
- Rovnanik, P., and Šafránková, K. (2016). Thermal behaviour of metakaolin/fly ash geopolymers with chamotte aggregate. *Materials* 9:535. doi: 10.3390/ma9070535
- Seabra, M. P., Labrincha, J. A., Novais, R. M., Buruberry, L. H., and Ascens, G. (2016). Porous biomass fly ash-based geopolymers with tailored thermal conductivity. *J. Clean. Prod.* 119, 99–107. doi: 10.1016/j.jclepro.2016.01.083
- Singh, B., Gupta, M., and Bhattacharyya, S. (2015). Geopolymer concrete: a review of some recent developments. *Constr. Build. Mater.* 85, 78–90. doi: 10.1016/j.conbuildmat.2015.03.036
- Siyal, A. A., Azizli, K. A., and Ullah, H. (2016). Effects of parameters on the setting time of fly ash based geopolymers using taguchi method. *Procedia Eng.* 148, 302–307. doi: 10.1016/J.PROENG.2016.06.624

- Strozi, M., Raymundo, M., and Colombo, P. (2014). Effect of process parameters on the physical properties of porous geopolymers obtained by gelcasting. *Ceram. Int.* 40, 13585–13590. doi: 10.1016/j.ceramint.2014.05.074
- Tchakoute, H. K., Elimbi, A., Yanne, E., and Djangang, C. N. (2013). Utilization of volcanic ashes for the production of geopolymers cured at ambient temperature. *Cement Concrete Compos.* 38, 75–81. doi: 10.1016/j.cemconcomp.2013.03.010
- Villaquirán-Cacedo, M., Mejía de Gutiérrez, R., and Gallego, N. C. (2017). A novel MK-based geopolymer composite activated with rice husk ash and KOH : performance at high temperature. *Mater. Constr.* 67, 1–13. doi: 10.3989/mc.2017.02316
- Vogt, O., Ukrainczyk, N., Steindlberger, E., and Koenders, E. A. B. (2016). *Geopolymerisation Activity of Eifel Tuff*. Available online at: <http://tubiblio.ulb-tu-darmstadt.de/81306/> (accessed October 17, 2018).
- Zhang, Z., Wang, H., Provis, J. L., Bullen, F., Reid, A., and Zhu, Y. (2012). Quantitative kinetic and structural analysis of geopolymers. Part 1. The activation of metakaolin with sodium hydroxide. *Thermochim. Acta* 539, 23–33. doi: 10.1016/j.tca.2012.03.021

Conflict of Interest Statement: The authors declare that the research was conducted in the absence of any commercial or financial relationships that could be construed as a potential conflict of interest.

Copyright © 2019 Bajare, Vitola, Dembovska and Bumanis. This is an open-access article distributed under the terms of the Creative Commons Attribution License (CC BY). The use, distribution or reproduction in other forums is permitted, provided the original author(s) and the copyright owner(s) are credited and that the original publication in this journal is cited, in accordance with accepted academic practice. No use, distribution or reproduction is permitted which does not comply with these terms.